Analysis of grain size effects on transformation-induced plasticity based on a discrete dislocation-transformation model

Shi, J.; Turteltaub, S.; Van der Giessen, E.

Published in:
Journal of the Mechanics and Physics of Solids

DOI:
10.1016/j.jmps.2010.07.021

Publication date:
2010

Journal of the Mechanics and Physics of Solids 58 (2010) 1863–1878

Contents lists available at ScienceDirect

Journal of the Mechanics and Physics of Solids

journal homepage: www.elsevier.com/locate/jmps

Analysis of grain size effects on transformation-induced plasticity based on a discrete dislocation–transformation model

J. Shi [a,1], S. Turteltaub [a,*], E. Van der Giessen [b]

[a] Faculty of Aerospace Engineering, Delft University of Technology, Kluyverweg 1, 2629 HS Delft, The Netherlands
[b] Zernike Institute for Advanced Materials, University of Groningen, Nijenborgh 4, 9747 AG Groningen, The Netherlands

ARTICLE INFO

Article history:
Received 19 November 2009
Received in revised form
26 July 2010
Accepted 27 July 2010

Keywords:
Discrete dislocation
Martensitic transformation
Size effect
Multiphase steel
Hall–Petch relation

ABSTRACT

There is much interest recently in the possibility of combining two strengthening effects, namely the reduction of grain size (Hall–Petch effect) and the transformation-induced plasticity effect (strengthening due to a martensitic transformation). The present work is concerned with the analysis of the combination of these two effects using a discrete dislocation–transformation model. The transformation-induced plasticity mechanism is studied for aggregates of grains of ferrite and austenite of different sizes. The discrete model allows to simulate the behavior at sub-grain length scales, capturing the complex interaction between pile-ups at grain boundaries and the evolution of the microstructure due to transformation. The simulations indicate that, as the average grain size decreases, the relative strengthening due to the formation of martensite is significantly reduced and that the overall strengthening is mostly due to a Hall-Petch effect. This finding suggests that strengthening by the transformation-induced plasticity mechanism is ineffective in the presence of fine-grained microstructures.

1. Introduction

Multiphase carbon steels exhibiting transformation-induced plasticity (or TRIP steels) have a good combination of strength and ductility and are well-suited for applications where both factors are important. These steels derive their overall mechanical characteristics from the properties of the individual phases present in the microstructure as well as from the interactions between the phases. A typical microstructure in a low-alloyed steel consists of high-carbon austenitic grains embedded in a ferrite-based matrix, which may also contain mixed-phase regions (in particular bainite) (Jacques, 2004). Upon mechanical loading (during forming or operation), the austenitic grains can partially or totally transform into martensite, which in multiphase steels is a harder phase in comparison to the parent austenitic phase. This phase transformation is accompanied by plastic deformation in the surrounding austenitic regions as well as in the ferritic matrix and gives rise to the transformation-induced plasticity effect. The coupling between plasticity and transformation is complex, often without a clear distinction between cause and effect, but the net effect is to increase the strength of the material in comparison with a non-transforming steel of similar composition. Understanding the details of this interaction is important in order to optimally utilize the transformation mechanism.

* Corresponding author. Tel.: +31 15 278 5360.
E-mail addresses: S.R.Turteltaub@tudelft.nl (S. Turteltaub), E.van.der.Giessen@rug.nl (E. Van der Giessen).
[1] Currently at: Huisman Equipment BV, Admiraal Trompstraat 2, 3115 HH Schiedam, The Netherlands.

0022-5096/$ - see front matter © 2010 Elsevier Ltd. All rights reserved.
doi:10.1016/j.jmps.2010.07.021

It is known that both the transformation mechanism as well as a reduction of grain size contribute to the increase in strength of a steel. An issue that has recently attracted attention in multiphase steels as well as fully-austenitic alloys is the combination of these two strengthening sources, i.e., the reduction in grain size of a steel assisted by transformation-induced plasticity. Grain size effects in ultra fine-grained, fully-austenitic alloys undergoing a martensitic phase transformation have been studied in Tao et al. (2007) and Yoo et al. (2008), where the increase in strength due to a reduction in grain size was observed in addition to the contribution of the transformation to the overall strengthening. In multiphase steels, the effect of grain size on the transformation behavior of austenitic grains was studied experimentally in Jimenez-Melero et al. (2007a,b) where it was found that smaller grains are more stable against transformation. One complication in the interpretation of these experimental results is that it is not simple to decouple the two strengthening sources, hence the individual contributions are difficult to establish.

Numerical simulations offer the possibility, through parametric analyses, to quantify the individual contributions to the strength of transformation and grain size. Grain size effects in multiphase steels have been recently analyzed through simulations performed in Turteltaub and Suiker (2006a) and Mazzoni-Leduc et al. (2008). The aforementioned analyses were based on a continuum description for the plastic deformations. However, since continuum models at sub-grain length scales cannot easily capture the complex interaction between pile-ups at grain boundaries and the evolution of the microstructure due to transformation, a discrete dislocation plasticity model is more appropriate in order to gain insight into the coupling between plasticity and transformation. The discrete dislocation method has been widely used to simulate grain size effects in single and polycrystalline samples (Biner and Morris, 2002, 2003; Nicola et al., 2005, 2006; Balint et al., 2006, 2008), but it has only recently been used in the context of phase transformation (Shi et al., 2008).

In the present contribution, the discrete transformation–dislocation model presented in Shi et al. (2008) is extended for the case of a multiphase material in order to study the influence of grain size on transformation-induced plasticity. The discrete transformation–dislocation model is applied to austenitic grains, while the discrete dislocation model is used to simulate the plastic flow in ferritic grains. Simulations are conducted in samples with different grain sizes and, for each grain size, with and without phase transformation to establish the relative strengthening contributions of the martensitic transformation and the reduction of grain size.

The paper is organized as follows: the constitutive models for transformation and plasticity in the distinct phases (austenitic/martensitic grains and ferritic grains) are summarized in Section 2. Material parameters for each phase and slip and transformation systems used in the simulations are given in Section 3. Parametric simulations are presented in Section 4, where the grain size of the ferritic and the austenitic phases are varied while keeping the same composition (i.e., same initial volume fractions). These parametric analyses provide valuable information on the role that the grain size has on the transformation-induced plasticity effect. Concluding remarks are presented in Section 5.

As a general scheme of notation, scalars are written as lightface italic letters, vectors as boldface lowercase letters (e.g., $\boldsymbol{a}$,$\boldsymbol{b}$) and second-order tensors as boldface capital letters (e.g., $\boldsymbol{A}$,$\boldsymbol{B}$) except for the stress and strain tensors for which boldface Greek letters are used. Fourth-order tensors are denoted using blackboard bold capital letters (e.g., $\mathbb{A}$, $\mathbb{B}$). The action of a second-order tensor upon a vector is denoted as $\boldsymbol{Ab}$ (in components, $A_{ij}b_j$ with implicit summation on repeated indices) and the action of a fourth-order tensor upon a second-order tensor is written as $\mathbb{A}\boldsymbol{B}$ (i.e., $A_{ijkl}B_{kl}$). The tensor product between two vectors is denoted as $\boldsymbol{a}\otimes\boldsymbol{b}$ (i.e., a_ib_j) and between two second-order tensors as $\boldsymbol{A}\otimes\boldsymbol{B}$ (i.e., $A_{ij}B_{kl}$). All inner products are indicated by a single dot between tensorial quantities of the same order (e.g., $\boldsymbol{a}\cdot\boldsymbol{b}$ and $\boldsymbol{A}\cdot\boldsymbol{B}$, i.e., a_ib_i and $A_{ij}B_{ij}$). Standard Miller index notation is used for crystallographic planes and directions with a subindex referring to the corresponding lattice basis. Super- and sub-script italic indices are typically used to refer to discrete entities (e.g., martenstic plates or dislocations) and super- and sub-script roman indices typically refer to the distinct phases (a, m and f for austenite, martensite or ferrite, respectively). Additional notation will be introduced where required.

2. Discrete dislocation–transformation model for multiphase steels

2.1. Decomposition

The method presented here is intended to analyze the response of a discrete aggregate of ferritic and austenitic grains. Upon loading, the austenite can transform into martensite, which appears in plate-like regions as shown schematically in Fig. 1. Following the approach developed in Shi et al. (2008), the stress, strain and displacement fields (denoted as $\boldsymbol{\sigma}$, $\boldsymbol{\varepsilon}$ and $\boldsymbol{u}$, respectively) are decomposed as follows:

$$\boldsymbol{\sigma}=\boldsymbol{\sigma}^{\mathrm{m}}+\boldsymbol{\sigma}^{\mathrm{d}}+\boldsymbol{\sigma}^{\mathrm{c}},\quad \boldsymbol{\varepsilon}=\boldsymbol{\varepsilon}^{\mathrm{m}}+\boldsymbol{\varepsilon}^{\mathrm{d}}+\boldsymbol{\varepsilon}^{\mathrm{c}},\quad \boldsymbol{u}=\boldsymbol{u}^{\mathrm{m}}+\boldsymbol{u}^{\mathrm{d}}+\boldsymbol{u}^{\mathrm{c}}, \tag{1}$$

where the superscripts m, d and c refer to the martensitic transformation problem, the dislocation problem and the so-called complementary problem, respectively. More specifically, suppose that at a given time t there are N^{m} plates of martensite and N^{d} dislocations in the system; the martensitic transformation problem consists of a collection of N^{m} problems, each one corresponding to an isolated plate of martensite embedded in an infinite austenitic matrix, and the dislocation problem refers to a collection of N^{d} problems, each one related to a single dislocation embedded in an infinite homogeneous medium (either ferrite, austenite or martensite depending on whether the dislocation core is located in the ferritic, austenitic or martensitic phase in the original problem, respectively). Consequently, the fields related to the

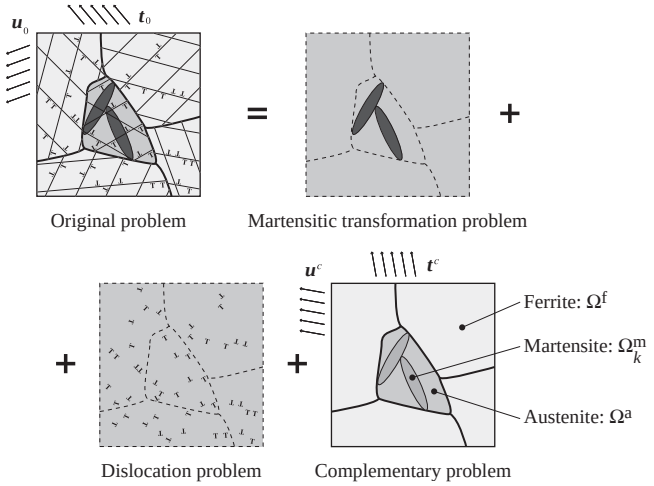

Fig. 1. Schematic decomposition of the original dislocation–transformation problem into three sub-problems for an aggregate of grains of ferrite and austenite.

transformation and dislocation problems are expressed as follows:

$$\boldsymbol{\sigma}^{\mathrm{m}} = \sum_{k=1}^{N^{\mathrm{m}}} \boldsymbol{\sigma}^{\mathrm{m}}_k, \quad \boldsymbol{\varepsilon}^{\mathrm{m}} = \sum_{k=1}^{N^{\mathrm{m}}} \boldsymbol{\varepsilon}^{\mathrm{m}}_k, \quad \boldsymbol{u}^{\mathrm{m}} = \sum_{k=1}^{N^{\mathrm{m}}} \boldsymbol{u}^{\mathrm{m}}_k, \tag{2}$$

$$\boldsymbol{\sigma}^{\mathrm{d}} = \sum_{i=1}^{N^{\mathrm{d}}} \boldsymbol{\sigma}^{\mathrm{d}}_i, \quad \boldsymbol{\varepsilon}^{\mathrm{d}} = \sum_{i=1}^{N^{\mathrm{d}}} \boldsymbol{\varepsilon}^{\mathrm{d}}_i, \quad \boldsymbol{u}^{\mathrm{d}} = \sum_{i=1}^{N^{\mathrm{d}}} \boldsymbol{u}^{\mathrm{d}}_i, \tag{3}$$

where quantities with subscripts k or i refer to the individual fields of a martensitic plate k or a dislocation i. Analytical expressions for the individual fields indicated in (2) and (3) in the case of martensitic plates with elliptical cross-sections and edge dislocations in an isotropic medium can be found in Shi et al. (2008) and Van der Giessen and Needleman (1995), respectively.

The tensor of elastic moduli of a phase p is denoted as $\mathbb{C}^p$, with p=f,a or m for the ferritic, austenitic or martensitic phases, respectively. For isotropic solids,

$$\mathbb{C}^p = \tfrac{1}{3}(3\kappa^p - 2\mu^p)\boldsymbol{I}\otimes\boldsymbol{I} + 2\mu^p\mathbb{I}, \tag{4}$$

where κ^p is the bulk modulus of phase p, μ^p is the shear modulus of phase p, and $\boldsymbol{I}$ and $\mathbb{I}$ are the second and fourth-order identity tensors, respectively. The region where the analysis is performed is denoted as Ω and the subregions occupied by a phase p are denoted as Ω^p. Further, the martensitic region Ω^{m} is subdivided into regions occupied by given plates $k \in [1,N^{\mathrm{m}}]$, which are denoted as Ω^{m}_k (see Fig. 1). The transformation fields $\boldsymbol{\sigma}^{\mathrm{m}}_k$ and $\boldsymbol{\varepsilon}^{\mathrm{m}}_k$ corresponding to a martensitic plate k are constitutively related as

$$\boldsymbol{\sigma}^{\mathrm{m}}_k = \begin{cases} \mathbb{C}^{\mathrm{a}}\boldsymbol{\varepsilon}^{\mathrm{m}}_k & \text{in } \Omega - \Omega^{\mathrm{m}}_k, \\ \mathbb{C}^{\mathrm{m}}(\boldsymbol{\varepsilon}^{\mathrm{m}}_k - \boldsymbol{\varepsilon}^{\mathrm{tr}}_k) & \text{in } \Omega^{\mathrm{m}}_k, \end{cases} \tag{5}$$

with the transformation strain $\boldsymbol{\varepsilon}^{\mathrm{tr}}_k$ being given by

$$\boldsymbol{\varepsilon}^{\mathrm{tr}}_k = \tfrac{1}{2}\gamma(\boldsymbol{m}^{\perp}_k\otimes\boldsymbol{m}_k + \boldsymbol{m}_k\otimes\boldsymbol{m}^{\perp}_k) + \delta(\boldsymbol{m}_k\otimes\boldsymbol{m}_k). \tag{6}$$

In (6), the vector $\boldsymbol{m}_k$ represents the normal to the (nominal) habit plane while $\boldsymbol{m}^{\perp}_k$ is a vector along the (nominal) habit plane (i.e., perpendicular to $\boldsymbol{m}_k$, see Fig. 2 and Shi et al., 2008 for further details). As indicated in (6), the transformation strain consists of an expansion of magnitude δ in the direction normal to the habit plane and a simple shear of magnitude γ parallel to the habit plane (symmetrized for consistency with the small strain theory). The orientation of the vector $\boldsymbol{m}_k$ is determined by the theory of martensitic transformations (Wechsler et al., 1953; Ball and James, 1987), i.e., it corresponds to one of the so-called *martensitic transformation systems* (see also Turteltaub and Suiker, 2006b).

The dislocation fields $\boldsymbol{\sigma}^{\mathrm{d}}_i$ and $\boldsymbol{\varepsilon}^{\mathrm{d}}_i$ related to a dislocation i are connected as

$$\boldsymbol{\sigma}^{\mathrm{d}}_i = \mathbb{C}^p\boldsymbol{\varepsilon}^{\mathrm{d}}_i \quad \text{for } i \in \mathcal{A}^p, \ p = \mathrm{f,a,m} \tag{7}$$

where the index p refers to the ferritic, austenitic or martensitic phase and $\mathcal{A}^p$ refers to the set of dislocations whose core is located within the phase p.

The complementary field, which is obtained numerically, is used to satisfy the actual boundary conditions and to account for the inhomogeneities due to the presence of a ferritic matrix as well as the formation and growth of martensitic

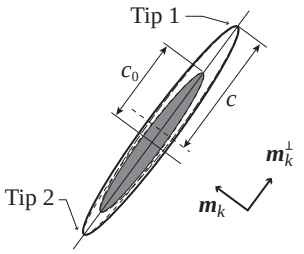

Fig. 2. Schematic representation of the growth of a martensitic plate inside an austenitic grain.

plates. Assuming quasi-static conditions, the original problem corresponds to solving $\operatorname{div}\boldsymbol{\sigma}=\mathbf{0}$ in Ω^*, together with the following stress–strain relations:

$$\boldsymbol{\sigma}=\begin{cases}\mathbb{C}^{\mathrm{f}}\boldsymbol{\varepsilon} & \text{in } \Omega^{\mathrm{f}*},\\ \mathbb{C}^{\mathrm{a}}\boldsymbol{\varepsilon} & \text{in } \Omega^{\mathrm{a}*},\\ \mathbb{C}^{\mathrm{m}}(\boldsymbol{\varepsilon}-\boldsymbol{\varepsilon}_k^{\mathrm{tr}}) & \text{in } \Omega_k^{\mathrm{m}*},\quad k=1,\ldots,N^{\mathrm{m}},\end{cases} \tag{8}$$

with $\boldsymbol{\varepsilon}=\frac{1}{2}(\nabla\boldsymbol{u}+\nabla\boldsymbol{u}^T)$ in Ω^* and prescribed displacement and/or traction boundary conditions. In (8), the regions $\Omega^*,\Omega^{\mathrm{f}*},\Omega^{\mathrm{a}*}$ and $\Omega_k^{\mathrm{m}*}$ refer to the corresponding domains $\Omega,\Omega^{\mathrm{f}},\Omega^{\mathrm{a}}$ and Ω_k^{m} but excluding the dislocation cores. In view of the decompositions (1)–(3), and the relations (5), (7) and (8), the complementary boundary value problem corresponds to solving $\operatorname{div}\boldsymbol{\sigma}^{\mathrm{c}}=\mathbf{0}$ in Ω^*, together with the following stress–strain relations:

$$\boldsymbol{\sigma}^{\mathrm{c}}=\begin{cases}\mathbb{C}^{\mathrm{f}}\boldsymbol{\varepsilon}^{\mathrm{c}}+\boldsymbol{P}_{\mathrm{f}}^{\mathrm{m}}+\boldsymbol{P}_{\mathrm{f}}^{\mathrm{d}} & \text{in } \Omega^{\mathrm{f}*},\\ \mathbb{C}^{\mathrm{a}}\boldsymbol{\varepsilon}^{\mathrm{c}}+\boldsymbol{P}_{\mathrm{a}}^{\mathrm{d}} & \text{in } \Omega^{\mathrm{a}*},\\ \mathbb{C}^{\mathrm{m}}\boldsymbol{\varepsilon}^{\mathrm{c}}+\boldsymbol{P}_k^{\mathrm{m}}+\boldsymbol{P}_k^{\mathrm{d}} & \text{in } \Omega_k^{\mathrm{m}*},\quad k=1,\ldots,N^{\mathrm{m}},\end{cases} \tag{9}$$

with $\boldsymbol{\varepsilon}^{\mathrm{c}}=\frac{1}{2}(\nabla\boldsymbol{u}^{\mathrm{c}}+(\nabla\boldsymbol{u}^{\mathrm{c}})^T)$ in Ω^* and prescribed boundary conditions for the complementary fields that follow from the boundary conditions of the original problem upon using (1)–(3). In (9), the tensors $\boldsymbol{P}_{\mathrm{f}}^{\mathrm{m}},\boldsymbol{P}_{\mathrm{f}}^{\mathrm{d}},\boldsymbol{P}_{\mathrm{a}}^{\mathrm{d}},\boldsymbol{P}_k^{\mathrm{m}}$ and $\boldsymbol{P}_k^{\mathrm{d}}$ are polarization stresses that result from the difference in elastic properties between the ferrite, austenite and martensite, given by

$$\boldsymbol{P}_{\mathrm{f}}^{\mathrm{m}}=(\mathbb{C}^{\mathrm{f}}-\mathbb{C}^{\mathrm{a}})\sum_{l=1}^{N^{\mathrm{m}}}\boldsymbol{\varepsilon}_l^{\mathrm{m}}, \tag{10}$$

$$\boldsymbol{P}_{\mathrm{f}}^{\mathrm{d}}=(\mathbb{C}^{\mathrm{f}}-\mathbb{C}^{\mathrm{a}})\sum_{j\in\mathcal{A}^{\mathrm{a}}}\boldsymbol{\varepsilon}_j^{\mathrm{d}}+(\mathbb{C}^{\mathrm{f}}-\mathbb{C}^{\mathrm{m}})\sum_{j\in\mathcal{A}^{\mathrm{m}}}\boldsymbol{\varepsilon}_j^{\mathrm{d}}, \tag{11}$$

$$\boldsymbol{P}_{\mathrm{a}}^{\mathrm{d}}=(\mathbb{C}^{\mathrm{a}}-\mathbb{C}^{\mathrm{f}})\sum_{j\in\mathcal{A}^{\mathrm{f}}}\boldsymbol{\varepsilon}_j^{\mathrm{d}}+(\mathbb{C}^{\mathrm{a}}-\mathbb{C}^{\mathrm{m}})\sum_{j\in\mathcal{A}^{\mathrm{m}}}\boldsymbol{\varepsilon}_j^{\mathrm{d}}, \tag{12}$$

$$\boldsymbol{P}_k^{\mathrm{m}}=(\mathbb{C}^{\mathrm{m}}-\mathbb{C}^{\mathrm{a}})\sum_{l=1,l\neq k}^{N^{\mathrm{m}}}\boldsymbol{\varepsilon}_l^{\mathrm{m}}, \tag{13}$$

$$\boldsymbol{P}_k^{\mathrm{d}}=(\mathbb{C}^{\mathrm{m}}-\mathbb{C}^{\mathrm{f}})\sum_{j\in\mathcal{A}^{\mathrm{f}}}\boldsymbol{\varepsilon}_j^{\mathrm{d}}+(\mathbb{C}^{\mathrm{m}}-\mathbb{C}^{\mathrm{a}})\sum_{j\in\mathcal{A}^{\mathrm{a}}}\boldsymbol{\varepsilon}_j^{\mathrm{d}}. \tag{14}$$

The subscripts f, a and k in (11)–(14) indicate that the polarization stresses are used to correct for the proper stiffness in the ferritic, austenitic or martensitic regions, respectively, while the superscripts m and d indicate whether the polarization stresses are related to the martensitic transformation or to the dislocation field, respectively.

2.2. Evolution of microstructure

Based on the stress state at time t, evolution relations are formulated to update the number and location of martensitic plates and dislocations from time t to time $t+\delta t$. The appearance of new dislocation dipoles and martensitic plates is simulated using nucleation points or sources randomly distributed across the specimen (dislocation sources in ferrite and austenite, and transformation sources in austenite). A dislocation source is connected to a specific slip system and may remain active to nucleate further dipoles. In contrast, a transformation source may potentially nucleate any crystallographically distinct transformation system, but once a martensitic plate has nucleated, the transformation source is no longer active.

At each transformation source k, all crystallographically distinct transformation systems are checked for possible nucleation by computing the driving force f_k^{nuc} based on an ideally flat interface that coincides with the corresponding

nominal habit plane of the transformation system. The transformation system for which f_k^{nuc} exceeds a critical value $f_k^{\mathrm{cr}} > 0$ is further tested based on an embryonic martensitic plate centered at the source and with a major semi-axis of length c_0 (see Fig. 2). The final criterion for actual nucleation is that this embryonic plate can grow, based on the growth criterion specified below. Embryonic plates that cannot grow are not allowed to nucleate; the source is monitored for possible nucleation during later times (see Shi et al., 2008 for details).

Growth of a martensitic plate is assumed to occur by lateral movement of the tips of the elliptical cross section along the (nominal) habit plane (i.e., major axis of cross section). In the present model, it is assumed that the aspect ratio of the martensitic plates, e, is preserved during growth. Consequently, the growth of the plate can be specified based on the velocities of the tips 1 and 2 along the direction of the vector $\boldsymbol{m}_k^{\perp}$, denoted as $v_{\mathrm{t}}^{(1)}$ and $v_{\mathrm{t}}^{(2)}$, respectively (see Fig. 2). The kinetic law that relates the velocity of tip q=1,2 to an effective transformation driving force is expressed as

$$v_{\mathrm{t}}^{(q)} = \frac{1}{B_{\mathrm{m}}(\pi e c)^2} \int_{S_k^{\mathrm{m}}} f_k^{\mathrm{tr}} w^{(q)} \, \mathrm{d}s \quad (q = 1,2), \tag{15}$$

where B_{m} is a drag coefficient for transformation, c is the current length of the major semi-axis, S_k^{m} is the interface between the martensitic plate and the austenite, and f_k^{tr} is the (local) transformation driving force at points on S_k^{m}. The weighting function $w^{(q)}$ varies from 1 at tip q to 0 at the opposite tip (see Shi et al., 2008 for details) as determined by the geometrical restriction of self-similar growth (i.e., growth with constant aspect ratio). The local transformation driving force f_k^{tr} corresponds to the jump in the Helmholtz energy across the interface minus the scalar product between the average traction and the jump in the strain vector. A specific form for f_k^{tr} that is convenient for the present method has been derived in Shi et al. (2008) as follows:

$$f_k^{\mathrm{tr}} = \boldsymbol{\sigma}^{\pm}\boldsymbol{n} \cdot \boldsymbol{\varepsilon}_k^{\mathrm{tr}}\boldsymbol{n} + \tfrac{1}{2}\,\mathbb{D}^{\mathrm{a}}\boldsymbol{\sigma}^{+} \cdot \boldsymbol{\sigma}^{+} - \tfrac{1}{2}\mathbb{D}^{\mathrm{m}}\boldsymbol{\sigma}^{-} \cdot \boldsymbol{\sigma}^{-} \quad \text{on } S_k^{\mathrm{m}}, \tag{16}$$

where $\boldsymbol{n}$ is the unit vector normal to the elliptical cross section, $\mathbb{D}^{\mathrm{a}} = (\mathbb{C}^{\mathrm{a}})^{-1}$ and $\mathbb{D}^{\mathrm{m}} = (\mathbb{C}^{\mathrm{m}})^{-1}$ are the compliance tensors of the austenite and martensite, respectively, and the superscript + (resp. $-$) indicates a quantity evaluated on the austenitic side (resp. martensitic side) of the austenite–martensite interface. The actual value of the tip velocity is limited by a cut-off value $v_{\max}^{\mathrm{m}}$ i.e., $0 \le v_{\mathrm{t}}^{(q)} \le v_{\max}^{\mathrm{m}}$ for q=1,2. Additional rules to handle special situations can be found in Shi et al. (2008).

Similarly, as proposed in Van der Giessen and Needleman (1995), nucleation of dislocation dipoles is modeled by two-dimensional Frank–Read sources. This process is controlled by the Peach–Koehler force, i.e. the driving force for dislocation motion. The Peach–Koehler force acting on a dislocation i is the shear component of the total stress at the current location of the dislocation (excluding the singular stress field $\boldsymbol{\sigma}_i^{\mathrm{d}}$ of the dislocation i itself), resolved on the slip system of that dislocation; that is,

$$f_i^{\mathrm{d}} = (\boldsymbol{\sigma} - \boldsymbol{\sigma}_i^{\mathrm{d}}) \cdot (\boldsymbol{b}_i \otimes \boldsymbol{n}_i), \tag{17}$$

where $\boldsymbol{n}_i$ is the slip plane normal and $\boldsymbol{b}_i$ the Burgers vector. A dislocation dipole is nucleated when the magnitude of the Peach–Koehler force at the location of a source exceeds a critical value $f^{\mathrm{cr}} = b\tau^{\mathrm{cr}}$ during a prescribed time interval t_{nuc}. Here, b is the magnitude of the Burgers vector and τ^{cr} is the strength of the dislocation source. After nucleation, the movement of each dislocation core i is determined by its velocity v_i^{d} along the slip direction, which is specified using the kinetic relation

$$v_i^{\mathrm{d}} = \frac{f_i^{\mathrm{d}}}{B_{\mathrm{d}}}, \quad 0 \le v_i^{\mathrm{d}} \le v_{\max}^{\mathrm{d}}, \tag{18}$$

where B_{d} is the drag coefficient for dislocation glide and $v_{\max}^{\mathrm{d}}$ is a cut-off value for the dislocation velocity. Additional details can be found in Van der Giessen and Needleman (1995). The nucleation criterion and kinetic law used for the ferrite and the austenite are formally similar (only the values of the model parameters are distinct). Experimental evidence indicates that the behavior of high-carbon martensite is mostly elastic until fracture, which occurs at high stress levels (see Jacques et al., 2006; Bowen et al., 1986). To take this into account, Frank–Read sources originally located in the austenitic phase that, due to a phase transformation, become embedded in the martensitic phase, are deactivated. Grain boundaries are incorporated in the simulation as impenetrable barriers for the movement of dislocations and, in the case of austenite–ferrite boundaries, as barriers for the growth of martensitic plates. Observe that grain boundaries between martensite and austenite may move due to growth of a martensitic plate and it is assumed that dislocations in the austenitic lattice are inherited in the martensitic phase. Dislocations that originally nucleated in the austenite and become trapped in martensite are subsequently modeled as immobile dislocations and their intrinsic stress field $\boldsymbol{\sigma}_i^{\mathrm{d}}$ is updated according to (7) (i.e., the stiffness is updated from $\mathbb{C}^{\mathrm{a}}$ to $\mathbb{C}^{\mathrm{m}}$ after transformation). However, for simplicity, the magnitude of the Burgers vector of the martensitic phase is taken equal to that of the austenitic phase. In addition, the elastic properties of the martensite and austenite are assumed to be such that their Poisson's ratio is the same, hence the intrinsic strain field $\boldsymbol{\varepsilon}_i^{\mathrm{d}}$ of a dislocation trapped in the martensite remains the same after transformation.

3. Slip systems, transformation systems and material parameters

At room temperature, ferrite has a BCC lattice structure and can contain only a limited amount of interstitial carbon, which makes it a softer phase in comparison with the carbon-rich austenitic phase. Austenite has an FCC lattice structure

and is primarily stable at high-temperatures. However, in low-alloyed multiphase steels (e.g., with the addition of elements such as Si or Al), austenite can remain as a metastable phase at room temperature (Jacques et al., 2001). Upon subsequent mechanical loading, austenite can transform into a relatively brittle high-carbon martenstic phase, which has a BCT lattice structure.

Slip in the austenitic FCC structure occurs primarily on the $\{1\,1\,1\}_a$ family of close-packed planes and in the $\langle 1\,1\,0\rangle_a$ directions. In the ferritic BCC structure, the most densely packed planes are $\{1\,1\,0\}_f$, while the main stacking-fault plane is $\{1\,1\,2\}_f$ (see, e.g., Hirth and Lothe, 1982). Plastic slip in BCC crystals operates mainly along the $\langle 1\,1\,1\rangle_f$ directions. Due to the lack of close-packed planes in BCC crystals, there is no clear consensus among researchers on which planes crystallographic slip occurs, though, experimentally, slip appears to occur mainly on the $\{1\,1\,0\}_f$ and $\{1\,1\,2\}_f$ planes. Simulations have suggested that glide on the $\{1\,1\,2\}_f$ planes is in fact composed of alternating short slip steps on the $\{110\}_f$ planes (see Vitek et al., 2004), although this is still a somewhat open issue. As mentioned in Section 2.2, the amount of plastic slip in high-carbon martensite is very limited and is not accounted for in the model.

The present simulations, however, are carried out within a plane strain setting, which implies that not all BCC and FCC slip systems are considered. In order to take the plane strain conditions into account, attention is restricted to the movement of edge dislocations whose lines lie in the out-of-plane direction of the specimens. To this end, the specimens are chosen such that the out-of-plane directions of the ferritic and austenitic grains are always $[1\,1\,0]_f$ and $[1\,1\,0]_a$, respectively. Based on the approach presented in Rice (1987), plastic deformation is assumed to occur by slip through the movement of edge dislocations on the $[1\,\overline{1}\,1]_f(\overline{1}\,1\,2)_f$ and $[\overline{1}\,1\,1]_f(1\,\overline{1}\,2)_f$ slip systems in the ferrite and the $[1\,\overline{1}\,2]_a(\overline{1}\,1\,1)_a$ and $[\overline{1}\,1\,2]_a(1\,\overline{1}\,1)_a$ slip systems in the austenite. Note that for the FCC systems, the slip direction is interpreted as an "effective" composite slip of equal amount along two slip directions in the slip plane (e.g., slip along the $[1\,\overline{1}\,2]_a$ direction on the $(\overline{1}\,1\,1)_a$ plane is a composite slip along the $[0\,\overline{1}\,1]_a$ and $[1\,0\,1]_a$ directions on the same plane). The slip plane normals of the $(\overline{1}\,1\,2)_f$ and $(1\,\overline{1}\,2)_f$ planes form an angle of approximately 60° between them. Similarly, there is an angle of approximately 60° between the slip plane normals of the $(\overline{1}\,1\,1)_a$ and $(1\,\overline{1}\,1)_a$ planes. The magnitude of the Burgers vector for ferrite and austenite is assumed to be the similar based on typical lattice parameters and actual slip.

The transformation systems found in an FCC austenite to BCT martensite transformation are not compatible with plane strain conditions (i.e., none of the habit plane vectors is perpendicular to the $[1\,1\,0]_a$ direction, see Turteltaub and Suiker, 2006b). For consistency with the plane strain formulation in the $(1\,1\,0)_a$ plane, two crystallographically distinct transformation systems are chosen for the simulations such that the vectors $\boldsymbol{m}_k$ and $\boldsymbol{m}_k^{\perp}$ (of each system) are perpendicular to the $[1\,1\,0]_a$ direction. The two distinct habit plane normal vectors $\boldsymbol{m}_k$ are chosen oriented at angles of 40° and 80° with respect to the austenitic slip plane normals mentioned above in order to mimic the actual three-dimensional angles between slip planes and habit planes (see Shi et al., 2008).

Here, for simplicity, the elastic properties of the ferrite and the austenite are assumed to be equal, $\mathbb{C}^f = \mathbb{C}^a$, which avoids the need to take polarization stresses into account related to the ferrite/austenite phases. However, the stiffness of martensite is taken to be 30% larger than that of austenite to model the strengthening due to the appearance of a harder phase after transformation. Although ferrite and austenite are assumed to have the same elastic moduli and, in the present plane strain setting, their slip planes are similarly spaced at 60° from each other, the plastic behavior of the two phases can be distinguished by the critical value for slip. The average dislocation source strength of the ferrite is taken to be about 90% of the average strength of the austenite. Specific values used for the onset of plastic slip as well as for the dislocation kinetic law are shown in Table 1 (see Shi et al., 2008 for details).

Table 1
Parameters for polycrystal simulations (overbars indicate the mean of the Gaussian distribution and SD the standard deviation).

Parameter(s)	Value(s)	Equation(s)
Elastic moduli		
Ferrite	$\kappa^f = 200\,\text{GPa}, \mu^f = 66.7\,\text{GPa}$	(4)
Austenite	$\kappa^a = 200\,\text{GPa}, \mu^a = 66.7\,\text{GPa}$	(4)
Martensite	$\kappa^m = 260\,\text{GPa}, \mu^m = 86.7\,\text{GPa}$	(4)
Transformation		
Strain	$\delta = 4\times10^{-3}, \gamma = 2\times10^{-2}$	(6)
Source strength	$\overline{f}^{cr}$ = 4 MPa, SD= 0.8 MPa	–
Embryonic plate	$c_0 = 0.1\,\mu\text{m}$, e=0.125	(15)
Kinetic law	$B_m = 10^8\,\text{Pa s m}^{-2}$, $v^m_{max} = 4800\,\text{m s}^{-1}$	(15)
Dislocation		
Burgers vector	b=0.25 nm	(17)
Strength ferrite	$\overline{\tau}^{cr} = 150\,\text{MPa}$, SD = 30 MPa, t^{nuc}= 10 ns	–
Strength austenite	$\overline{\tau}^{cr} = 170\,\text{MPa}$, SD = 34 MPa, t^{nuc}=10 ns	–
Kinetic law	$B_d = 10^{-4}\,\text{Pa s}, v^d_{max} = 20\,\text{m s}^{-1}$	(18)

Unless explicitly indicated, dislocation parameters for the ferrite and austenite are taken equal to each other.

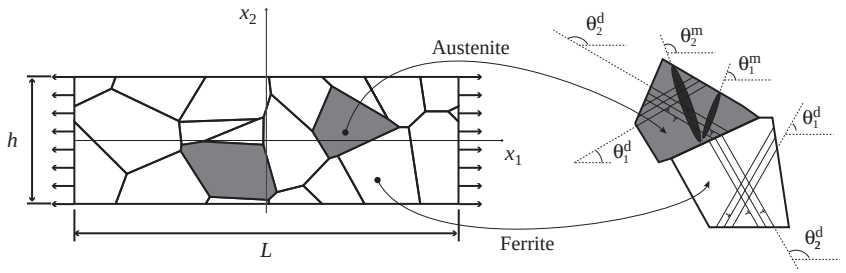

Fig. 3. Typical sample geometry and orientation of slip and transformation systems in austenitic and ferritic grains.

Table 2
Orientation of slip and transformation systems (angles are measured anti-clockwise with respect to the sample's x_1 loading axis, see inset Fig. 3).

	θ_1^d (deg)	θ_2^d (deg)	θ_1^m (deg)	θ_2^m (deg)
Austenite	30	150	70	110
Ferrite	60	120	–	–

Values for the material parameters of the transformation model are also included in Table 1. It is noted that the transformation strain parameters δ and γ are scaled values of the actual crystallographic values (scaled by a factor of 0.1) in order to keep the stress level within representative values while limiting the number of dislocations that nucleate in the simulations to a manageable range. In order to study the strengthening due to the martensitic transformation and grain size, other mechanisms are not included in the simulations (e.g., the specimens contain no dislocation obstacles except for grain boundaries, habit planes that appear during the simulation and constrained external boundaries). It is worth mentioning that the critical values for nucleation of dislocation dipoles and martensitic plates, as shown in Table 1, differ by up to two orders of magnitude. However, this difference is only related to the expressions used for the plastic and transformation driving forces, as given in (16) and (17), which are scaled differently. The actual stresses at which the transformation and dislocation sources are activated are of the same order of magnitude.

In all simulations, a rectangular sample with in-plane dimensions $L=12\,\mu$m and $h=4\,\mu$m is subjected to plane-strain uniaxial deformation by imposing the following boundary conditions:

$$u_1(x_1=\pm L/2,x_2,t)=\pm\tfrac{1}{2}L\dot{\bar{\varepsilon}}_{11}t,\quad u_2(x_1=\pm L/2,x_2,t)=0, \tag{19}$$

$$\sigma_{12}(x_1,x_2=\pm h/2,t)=0,\quad \sigma_{22}(x_1,x_2=\pm h/2,t)=0, \tag{20}$$

with a nominal strain rate $\dot{\bar{\varepsilon}}_{11}=(1/6)\times 10^4\,\mathrm{s}^{-1}$ for extension, as shown in Fig. 3. The left and right sides of the specimen ($x_1=\pm L/2$) are taken to be impenetrable boundaries for dislocations. The top and bottom sides of the samples ($x_2=\pm h/2$) are modeled as free boundaries so that dislocations can move out of the specimen there, leaving a slip step. The in-plane orientation of the austenitic and ferritic grains is such that the slip and transformation systems are as indicated in Table 2 (see also Fig. 3). All grains of a given phase have the same orientation; this simplification is adopted since it was found in Balint et al. (2008) that the dependence of the flow strength on grain size is observed even in the absence of slip incompatibility across grain boundaries. In all simulations, the initial specimens comprise an aggregate of ferritic and untransformed austenitic grains with zero residual stress and without any mobile dislocation.

4. Grain size effect on transformation-induced plasticity

4.1. Simulations

To study the influence of the austenitic and ferritic grain sizes, simulations are carried out for samples with different grain sizes while keeping the dislocation source density constant. Nine samples consisting of an aggregate of austenitic and ferritic grains were generated using a Voronoi algorithm. All samples have an approximate initial austenitic volume fraction $\xi_0^a=15\%$. These samples are divided into three groups based on similar average grain sizes for the ferritic and austenitic grains, as shown in Fig. 4. Table 3 lists the representative size of the grains in each phase, calculated as $d^p=\sqrt{A_p/N_p^G}$, where A_p is the area occupied by grains of phase p and N_p^G is the number of grains of phase p.

Dislocation sources in the ferrite and austenite are randomly distributed on slip planes spaced $200b$ apart and each source is randomly assigned a nucleation strength from a Gaussian distribution as indicated in Section 2.2 with parameters given in Table 1. The dislocation source density is approximately $17\,\mu\mathrm{m}^{-2}$ in the ferritic grains and $10\,\mu\mathrm{m}^{-2}$ in the

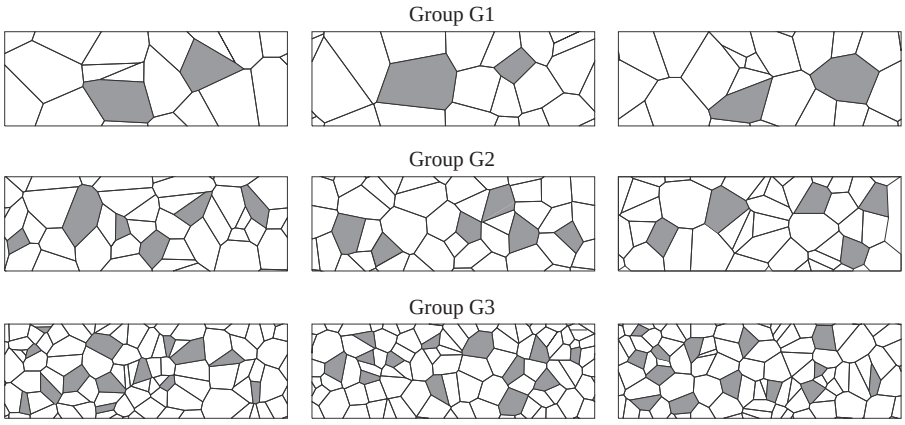

Fig. 4. Sample geometries for each group. Austenitic grains are shown in gray.

Table 3
Average representative grain size $\overline{d}^p$ of phase p for samples of groups G1, G2 and G3.

Group	G1	G2	G3
$\overline{d}^{\mathrm{a}}$ (austenite) (μm)	1.91	1.12	0.72
$\overline{d}^{\mathrm{f}}$ (ferrite) (μm)	1.34	0.96	0.68

austenitic grains. The location and strength of the transformation sources in the austenite are distributed in a similar way with source densities of approximately 17, 43 and 102 μm^{-2} for groups G1, G2 and G3, respectively. Preliminary numerical simulations indicate that the transformation behavior is not very sensitive to the transformation source density for sufficiently large densities. The transformation source densities indicated above were chosen accordingly (i.e., such that the transformation behavior did not vary significantly with an increase in transformation source density).

In order to quantify the relative contribution of the transformation mechanism on the effective hardening, two types of simulations are considered for each sample, namely

- A dislocation-only simulation where the transformation sources are suppressed and the material only deforms plastically.
- A combined transformation–dislocation simulation where both plasticity and transformation are active.

4.2. Results

The average axial stresses $\overline{\sigma}_{11}$ (averaged over the whole sample) as a function of the average axial strain $\overline{\varepsilon}_{11}$ are presented in Fig. 5 for each grain size group (indicated in black, gray and light gray corresponding to groups G1, G2 and G3, respectively). Combined transformation–dislocation simulations are represented by solid lines, while dislocation-only simulations are represented by dashed lines. The stress–strain response of each group corresponds to an average value of the three samples in the group.

For the combined dislocation–transformation simulation, the partitioning of stress within phases is shown in Fig. 6 as a function of the average axial strain (averaged over the whole domain). Here, the phase-averaged axial stresses are computed as follows:

$$\overline{\sigma}^{\mathrm{f}}_{11} = \frac{1}{|\Omega^{\mathrm{f}}|}\int_{\Omega^{\mathrm{f}}} \sigma_{11}\,\mathrm{d}a, \quad \overline{\sigma}^{\mathrm{a,m}}_{11} = \frac{1}{|\Omega^{\mathrm{a}} \cup \Omega^{\mathrm{m}}|}\int_{\Omega^{\mathrm{a}}\cup\Omega^{\mathrm{m}}} \sigma_{11}\,\mathrm{d}a,$$

where $\overline{\sigma}^{\mathrm{f}}_{11}$ is the axial stress averaged in the ferritic grains, $\overline{\sigma}^{\mathrm{a,m}}_{11}$ is the axial stress in the austenitic grains (that can partially transform into martensite), $\Omega^{\mathrm{a}} \cup \Omega^{\mathrm{m}}$ corresponds to the region where the material is either in the austenitic or martensitic phase and the vertical bars indicate the area of the corresponding region.

The evolution of dislocation density, for each type of simulation and each grain size group, is shown in Fig. 7(a) for dislocations in the ferritic matrix and in Fig. 7(b) for dislocations in the austenitic phase. The evolution of the austenitic

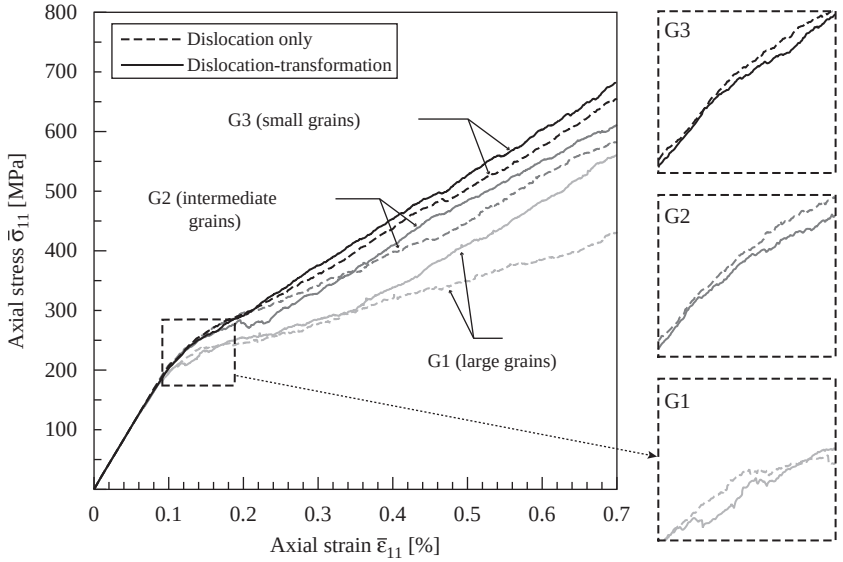

Fig. 5. Average axial stress $\overline{\sigma}_{11}$ as a function of the average axial strain $\overline{\varepsilon}_{11}$ for three distinct grain sizes and for simulations without and with the transformation mechanism (i.e., dislocation-only and dislocation–transformation simulations).

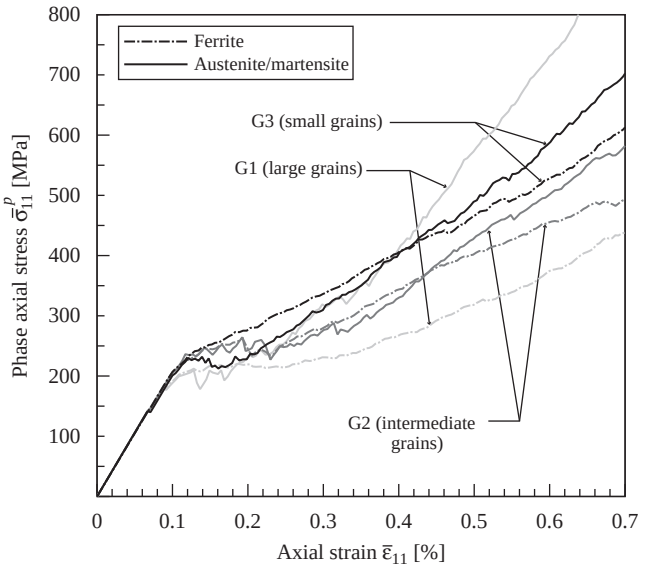

Fig. 6. Axial stress $\overline{\sigma}_{11}^{p}$ averaged over austenitic/martensitic grains and ferritic grains as a function of the average axial strain $\overline{\varepsilon}_{11}$ for three distinct grain sizes according to the dislocation–transformation computation.

volume fraction ξ^{a} (normalized by the initial austenitic volume fraction ξ_0^{a}) is shown in Fig. 8 as a function of the average axial strain $\overline{\varepsilon}_{11}$ for the three distinct groups of grain sizes.

In addition to the results presented above, it is useful to analyze in more detail the distribution of stress and plastic slip in the samples. Moreover, in order to quantify the accumulated effect of discrete dislocations, one can introduce a (continuum) decomposition of the total strain $\boldsymbol{\varepsilon}$ as

$$\boldsymbol{\varepsilon} = \boldsymbol{\varepsilon}^{e} + \boldsymbol{\varepsilon}^{tr} + \boldsymbol{\varepsilon}^{p}, \tag{21}$$

into the elastic strain $\boldsymbol{\varepsilon}^{e}$, transformation strain $\boldsymbol{\varepsilon}^{tr}$ and plastic strain $\boldsymbol{\varepsilon}^{p}$. A discrete dislocation simulation provides the stress $\boldsymbol{\sigma}$ and the displacement $\boldsymbol{u}$ according to the decompositions $(1)_1$ and $(1)_3$. Although in principle the total strain $\boldsymbol{\varepsilon}$ can be obtained from $(1)_2$, in practice it can be more conveniently computed numerically from the displacement field as $\boldsymbol{\varepsilon} = (1/2)(\nabla \boldsymbol{u} + \nabla \boldsymbol{u}^{T})$. In the context of a finite element method, the total strain $\boldsymbol{\varepsilon}$ contains information about the *average* displacement jumps across the

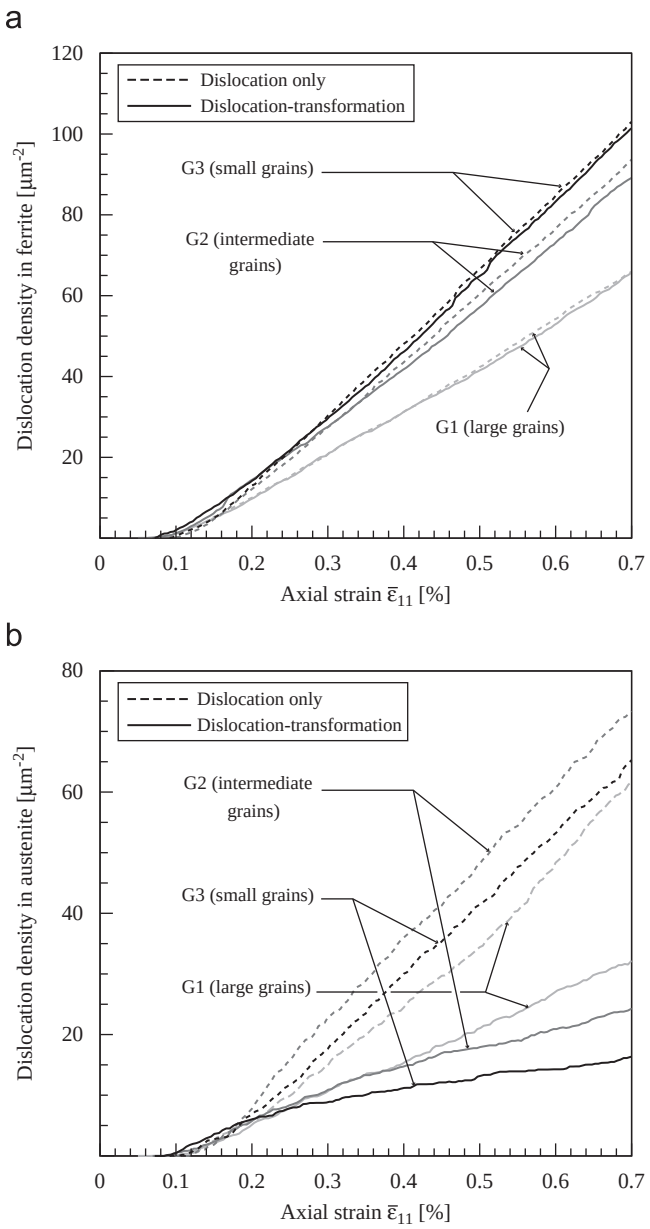

Fig. 7. Dislocation density in (a) ferrite and (b) austenite as a function of the average axial strain $\bar{\varepsilon}_{11}$ for three distinct grain sizes and for each type of simulation (i.e., without and with transformation).

slip planes contained within each element. The transformation strain $\boldsymbol{\varepsilon}^{\mathrm{tr}}$ can be determined as

$$\boldsymbol{\varepsilon}^{\mathrm{tr}} = \begin{cases} \mathbf{0} & \text{in } \Omega - \Omega_k^{\mathrm{m}}, \\ \boldsymbol{\varepsilon}_k^{\mathrm{tr}} & \text{in } \Omega_k^{\mathrm{m}}, \end{cases} \tag{22}$$

where $\boldsymbol{\varepsilon}_k^{\mathrm{tr}}$ is the transformation strain associated with the martensitic plate Ω_k^{m}, as given in (6). The elastic strain can be computed from the stress as

$$\boldsymbol{\varepsilon}^{\mathrm{e}} = \mathbb{D}^p \boldsymbol{\sigma}, \tag{23}$$

where $\mathbb{D}^p = (\mathbb{C}^p)^{-1}$ is the compliance tensor of phase p=f,a or m for the ferritic, austenitic or martensitic phases, respectively. Consequently, the (continuum) plastic strain can be obtained from (21) to (23). In line with crystal plasticity theory, the plastic

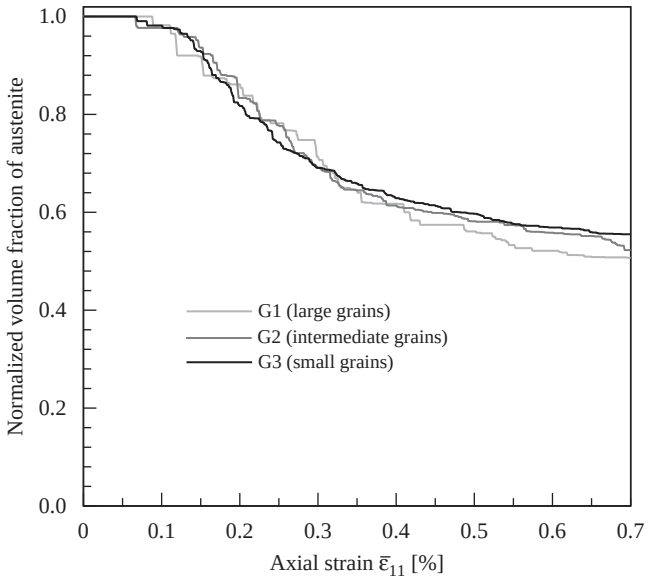

Fig. 8. Normalized austenitic volume fraction ξ^a/ξ_0^a as a function of the average axial strain $\bar{\varepsilon}_{11}$ for three distinct grain sizes.

strain can be viewed in terms of the accumulated plastic slip $\gamma^{(\alpha)}$ on a slip system α as

$$\boldsymbol{\varepsilon}^p = \sum_{\alpha=1}^{N} \gamma^{(\alpha)} \boldsymbol{s}^{(\alpha)} \otimes \boldsymbol{n}^{(\alpha)}, \tag{24}$$

where $\boldsymbol{s}^{(\alpha)}$ is the tangent vector and $\boldsymbol{n}^{(\alpha)}$ is the normal vector to slip system α. Several scalar measures can be used to quantify the plastic slip, such as the norm of the plastic strain tensor $\|\boldsymbol{\varepsilon}^p\|$. Here, the measure Γ used in Balint et al. (2008), referred to as equivalent plastic slip, is used for that purpose. The equivalent plastic slip is defined as

$$\Gamma \coloneqq \sum_{\beta=1}^{N} |\boldsymbol{s}^{(\beta)} \cdot \boldsymbol{\varepsilon}^p \boldsymbol{n}^{(\beta)}| = \sum_{\beta=1}^{N} \left| \sum_{\alpha=1}^{N} \gamma^{(\alpha)} (\boldsymbol{s}^{(\alpha)} \cdot \boldsymbol{s}^{(\beta)})(\boldsymbol{n}^{(\alpha)} \cdot \boldsymbol{n}^{(\beta)}) \right|, \tag{25}$$

where the right hand side of (25) follows from (24). The distributions of equivalent plastic slips Γ in samples with different representative grain sizes for simulations with and without transformation are shown in Figs. 9 and 10, respectively. The samples depicted in these figures correspond to the middle column in Fig. 4. The distribution of axial stresses σ_{11} for the combined dislocation–transformation simulation is shown in Fig. 11.

The results shown in Figs. 5–11 are analyzed in the subsequent subsections in terms of the following:

1. The transformation-induced plasticity effect, which can be assessed by comparison of simulations without and with transformation for a given grain size.
2. The grain size effect (i.e., grain size dependence analyzed for each type of simulation separately).
3. The interaction between these two hardening mechanisms (i.e., transformation-induced plasticity effect as a function of grain size and, conversely, the influence of transformation on the Hall–Petch effect).

4.3. Transformation-induced plasticity effect

Comparison of the stress–strain responses shown in Fig. 5 with and without transformation reveals that, for all groups, the stress level is initially lower in the dislocation–transformation case than in the dislocation-only case (see inset in Fig. 5). Although the difference is relatively small, all individual simulations showed consistently the same trend. This is due to the additional relaxation capacity provided by the transformation mechanism compared to plastic deformation only (i.e., more energy can be instantaneously dissipated by combining two inelastic mechanisms, namely transformation and plastic deformation, see also Shi et al., 2008). However, as the strain increases, the stress response in the presence of transformation rises above that without transformation (for all groups), which indicates a higher strength and work hardening rate associated to the martensitic transformation. The appearance of martensite eventually endows the material with higher strength due to its higher stiffness and elastic response. These trends are consistent with simulations of a single crystal of austenite reported in Shi et al. (2008) and, in general, with the transformation-induced plasticity effect (Turteltaub and Suiker, 2005; Suiker and Turteltaub, 2005; Tjahjanto et al., 2006, 2007, 2008).

The strain at which the material starts to yield plastically (measured in terms of an increase in dislocation density in Figs. 7(a) and (b) and the strain at which the austenite starts to transform (measured in terms of a decrease in austenitic volume fraction in Fig. 8) are somewhat similar, both slightly smaller than 0.1%. A detailed analysis of the data for the simulations with transformation reveals that the onset of transformation occurs shortly after the onset of plastic deformation. The two

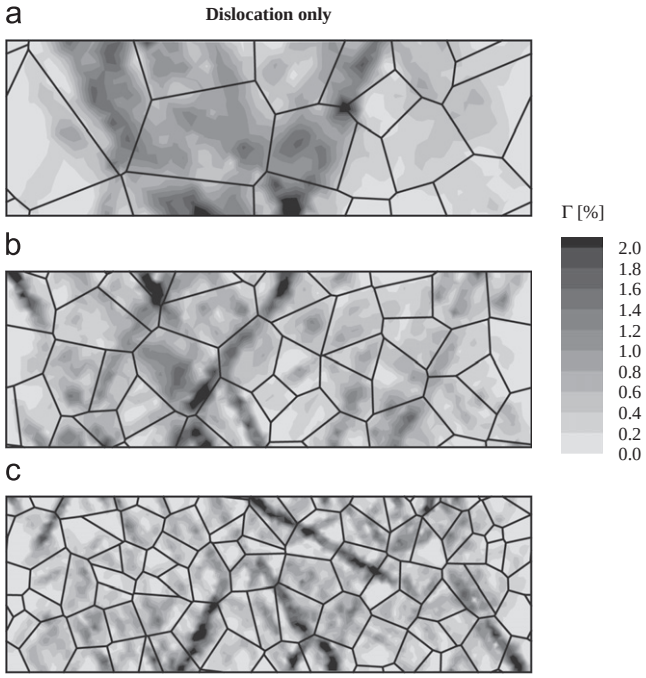

Fig. 9. Contour plot of equivalent plastic slip Γ for the dislocation-only simulation at an average axial strain $\bar{\varepsilon}_{11} \approx 0.5\%$ in typical samples from (a) group G1 (large grains), (b) group G2 (intermediate grains) and (c) group G3 (small grains).

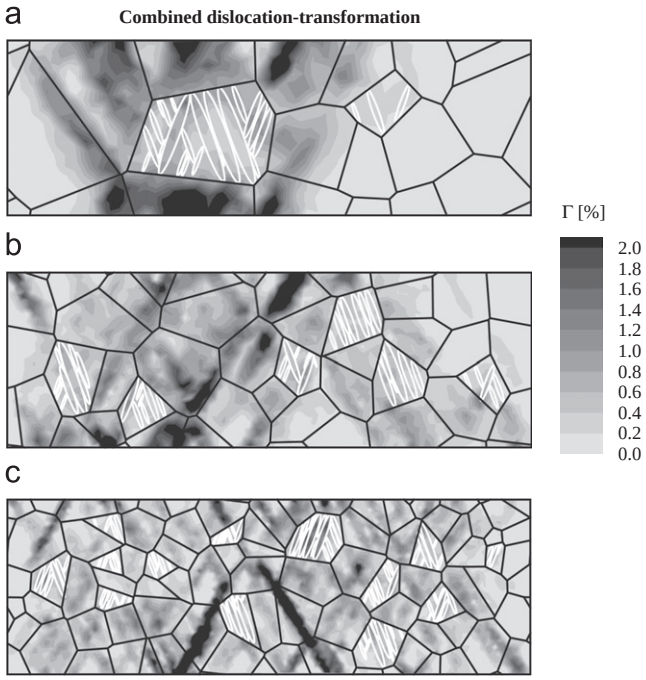

Fig. 10. Contour plot of equivalent plastic slip Γ for the dislocation–transformation simulation at an average axial strain $\bar{\varepsilon}_{11} \approx 0.5\%$ in typical samples from (a) group G1 (large grains), (b) group G2 (intermediate grains) and (c) group G3 (small grains). The boundaries of the current martensitic plates are indicated in white.

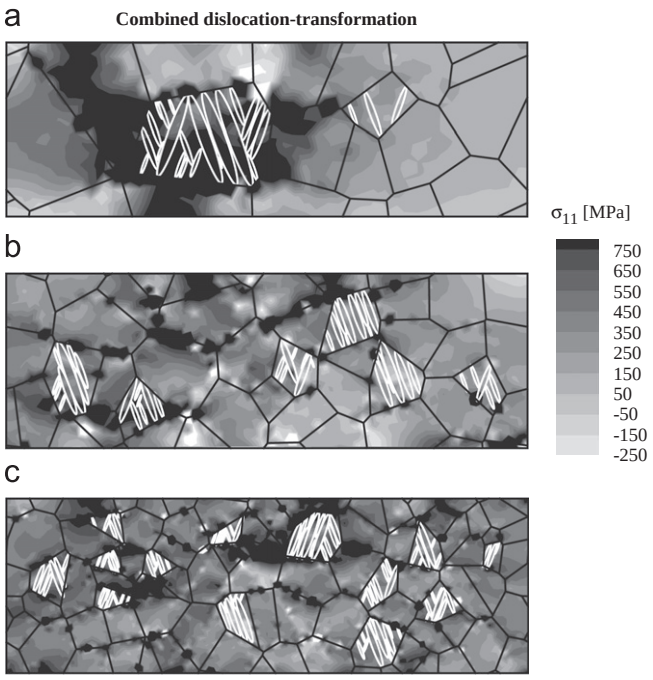

Fig. 11. Contour plot of axial stress σ_{11} for the dislocation–transformation simulation at an average axial strain $\overline{\varepsilon}_{11} \approx 0.5\%$ in typical samples from (a) group G1 (large grains), (b) group G2 (intermediate grains) and (c) group G3 (small grains). The boundaries of the current martensitic plates are indicated in white.

mechanisms remain active until eventually the transformation rate becomes small due to a gradual depletion of available austenite (see Fig. 8). During the first stage of deformation, while the material is transforming, the hardening rate is dominated by the plastic hardening mechanism (i.e., the stress–strain response shown in Fig. 5 is similar for the simulations without and with transformation). After the transformation process is completed (i.e., small transformation rate in Fig. 8), the hardening rate is strongly connected to the behavior of the hard martensitic phase that has appeared in the austenitic grains. This effect is most noticeable for group G1 in Fig. 5, where the deviation between the simulations without and with transformation becomes significant when the transformation process slows down at a strain of around 0.3%.

The effect of transformation on the plastic response can be further analyzed by studying the evolution of dislocation density shown in Fig. 7. A detailed analysis of the results at the onset of plastic deformation reveals that initially the number of dislocations for the simulation with transformation is *larger* than that of the dislocation-only simulation. However, as the strain increases, the density of dislocations in the austenite (and to a lesser degree in the ferrite) for the combined dislocation–transformation simulation is *smaller* than in the dislocation-only simulation (see Fig. 7). The initially higher number of dislocations for the simulation with transformation is related to the plastic accommodation of the transformation strain, which occurs both in the adjacent austenitic regions inside a partially transformed grain as well as in the surrounding ferritic matrix. One might expect a priori that this accommodation mechanism remains active upon continued straining, so that the dislocation density in the simulations with transformation would remain higher. However, the number of dislocations for the simulation with transformation eventually becomes *less* than for the simulation without transformation, a phenomenon that deserves a clarification. This effect can be observed in more detail by comparing Figs. 9 and 10, which depict the distribution of equivalent plastic slip Γ in typical samples from groups G1, G2 and G3 at an average axial strain $\overline{\varepsilon}_{11} \approx 0.5\%$ for the simulations without and with transformation. A comparison between similar regions in Figs. 9 and 10 reveals that the ferritic and austenitic grains experience indeed less plastic deformation in the combined dislocation–transformation simulation than in the plasticity-only simulation. In particular, in view of the stress distribution shown in Fig. 11, less plastic deformation in the *ferrite* is observed in regions under the influence of the compressive transformation field (i.e., the transformation relaxes the externally applied tensile stress in areas away from the tips of the adjacent martensitic plates, hence less dislocations sources are activated). In the *austenite*, less plastic deformation is observed in the presence of a phase transformation than without it since, in addition to the stress relaxation associated to the transformation, there is effectively *less* austenite as the transformation proceeds (and thus less dislocation sources), hence less plastic deformation is generated in the combined dislocation–transformation simulation.

It is worth pointing out that in the simulations for an austenitic single crystal presented in Shi et al. (2008), it was found that the number of dislocations in the austenite for the combined transformation–dislocation simulations was *higher* than the dislocation-only simulations, which is the opposite behavior as observed in the present work. This apparent discrepancy can be traced back to the fact that the single crystal austenitic specimen analyzed in Shi et al. (2008) has an

abundance of free boundaries across which dislocations can leave the specimen, whereas the austenitic grains analyzed here are more representative of bulk behavior. Indeed, in the single crystal simulations analyzed in Shi et al. (2008), it was found that the martensitic plates played a role similar to grain boundaries in the sense that they acted as barriers for the movement of dislocations. This explained that more dislocations were observed in the simulations with transformation than in the dislocation-only simulations. In contrast, in the present work all austenitic grains are fully embedded in a ferritic matrix, so that the preferred mechanism to eliminate dislocations (i.e., escaping through a free boundary) is no longer available. Furthermore, the stress relaxation due to the transformation and the corresponding reduction of available austenite that can deform plastically compensates for the additional dislocations generated due to internal pile ups in the austenitic grains. Hence the net effect of these competing mechanisms is that fewer dislocations are observed in the austenitic phase for the simulations with transformation than for the simulations without transformation.

4.4. Hall–Petch effect

Hall (1951) and Petch (1953) first correlated the macroscopic yield strength σ in mild steels with the inverse square root of the grain size d, i.e., $\sigma = \sigma_0 + kd^{-1/2}$, where σ_0 is the limiting large-grain yield strength and k a material parameter. Although the Hall–Petch relation was originally proposed to correlate the *initial* yield strength with grain size, similar relations have been used subsequently to incorporate hardening, with σ_0 and k viewed as functions that depend on some strain measure. The power 1/2, however, then is not always the best fit. A more general view is that the flow strength of steels of similar composition and subjected to the same deformation will scale as d^{-n}, with n ranging typically between 1/3 and 1, as reported in Kocks (1970a,b), Ashby (1970), and Hirth (1972).

A variety of microscale models have been proposed to explain the Hall–Petch relation. Eshelby et al. (1951) and Hirth and Lothe (1982) proposed that dislocation pile-ups at grain boundaries scale with the grain size, and that stress concentrations associated with these pile-ups give rise to the dependence of σ on the inverse square root of d. Another model is based on the experimental correlation of flow stress with dislocation density (see Embury, 1971). Balint et al. (2006, 2008) carried out two-dimensional discrete dislocation simulations with different dislocation source densities and slip incompatibility between grains in thin films and in periodic samples. For both types of polycrystal samples under uniaxial deformation, they predicted that the flow strength increased with decreasing *grain size*, i.e., a Hall–Petch effect. Moreover, they found that the strengthening with decreasing grain size depends mainly on slip transmission across grain boundaries (for large dislocation source densities) or slip blockage (for low dislocation source densities). Furthermore, the grain size effect was obtained even in the absence of slip incompatibility across grain boundaries.

Relative to the values used by Balint et al. (2006, 2008), the present simulations are carried out with *low* dislocation source densities. Preliminary simulations (not shown here), which were performed using the same geometries as the ones presented in Fig. 4 but consisting *only* of *ferritic* grains have indicated that the initial yield strength depends on the ferritic grain size as $d^{-2/3}$, which is within the typical range of values that the exponent of d can assume. Due to the increase of internal boundaries as the grain size decreases, more dislocations pile-up along the boundaries. Consequently, dislocation pile-ups cause more generation of dislocation dipoles, consistent with the findings indicated in Balint et al. (2006, 2008).

For the multiphase case (ferrite and austenite) comparing the curves of the dislocation-only simulations shown in Fig. 5 (dashed lines) of groups G1, G2 and G3, it can be seen that a reduction of the average grain size results in a higher stress and work hardening rate, which is again consistent with the trends associated with the Hall–Petch effect. Within the range of grain sizes analyzed here, the grain boundaries in samples with smaller grains do not fully prevent the formation of shear bands (see Fig. 9(c)). However, in general, the plastic deformation is more evenly distributed in samples with smaller grains than in samples with larger grains (see, e.g., Figs. 9(a) and (c)).

Similar to the dislocation-only case, in the combined dislocation–transformation simulations (solid lines in Fig. 5), the yield strength and hardening rate increase with decreasing grain size. However, when resolved per phase, the trend is not the same for the ferrite and the austenite/martensite. Although a Hall–Petch effect can be observed in the ferritic grains (dashed lines in Fig. 6), the yield strength in the austenite/martensite grains does not depend monotonically on grain size (solid lines in Fig. 6). In fact, for sufficiently large axial deformations, the largest phase-average stress occurs in samples with large grains, which is the opposite of the classical Hall–Petch effect. A similarly unexpected relation can be observed in the dislocation densities as a function of axial strain as depicted in Fig. 7(a) (averaged over the ferritic grains) and Fig. 7(b) (averaged over the austenitic/martensitic grains). Consistent with the pile-up-based explanation of the Hall–Petch effect, Balint et al. (2006, 2008) observed that the dislocation density at a given strain decreases with grain size in a similar fashion as the yield strength does. In the combined dislocation–transformation simulations here, the dislocation density in the ferrite indeed increases with decreasing grain size, but in the austenite/martensite it shows the opposite trend, i.e., it decreases with decreasing grain size. An explanation for this unusual behavior is provided in the next subsection.

4.5. Interaction between hardening mechanisms

A question of practical interest is to quantify the effect of simultaneously using the two hardening sources indicated in the preceding sections, i.e., the purpose is to determine whether a reduction of grain size in a steel assisted by transformation-induced plasticity would result in a substantially improved hardening behavior. The results shown in Fig. 5

indicate that although the transformation mechanism always provides more strength compared to a specimen that can only deform plastically, the contribution of the transformation mechanism becomes smaller as the grain size decreases. Consequently, it could be concluded that the strengthening associated to the martensitic transformation becomes less significant than the strengthening associated to the Hall–Petch effect as the grain size decreases.

Regarding the stress distribution shown in Fig. 11(a), for samples with larger grains, the stress concentrates in and around the austenitic grains that have transformed into martensite. Ferritic grains that are further apart from the austenitic grains show low stress levels. For samples with smaller grains, more stress concentrates at grain boundaries (due to dislocation pile-ups) but, in general, the stress is more evenly distributed than for samples with larger grains (compare Figs. 11(a) and (c)). It is interesting to observe that the stress in the *austenitic* grains that have (partially) transformed into martensite is lower in samples with smaller grains than with larger grains. Indeed, the relative stress partitioning between ferritic and austenitic/martensitic grains depends strongly on grain size. From Fig. 6, which shows the axial stress averaged over the distinct phases as a function of the overall axial strain, it can be observed that the austenitic/martensitic grains carry an increasingly larger percentage of the total load as the grain size increases. Conversely, smaller ferritic grains have an increased load-carrying capacity as the grain size decreases.

The fact that less load is carried by the austenitic grains (relative to the ferritic grains) as the grain size decreases, explains that the hardening due to the transformation mechanism becomes *less efficient* as the grain size decreases (i.e., the increased stiffness connected to the hard martensitic phase is used less efficiently since the austenitic/martensitic grains carry relatively less load). This phenomenon also clarifies the evolution of dislocation densities observed in the austenite for different grains sizes. Indeed, since austenitic/martensitic grains carry preferentially more load for larger grain sizes, then the higher local stresses in those grains trigger more plastic deformation in the untransformed austenite than in samples with smaller grain sizes.

5. Concluding remarks

The parametric study of polycrystalline samples of multiphase steels assisted by transformation-induced plasticity using a discrete transformation–dislocation model has shown the influence of various microstructural characteristics on their overall mechanical behavior. Despite the limitations of a small strain range and plane strain analysis and the need to simplify some features in the model (e.g., elastic isotropy and fixed morphology for the martensitic plates), the main advantage of the present formulation is to retain the discrete character of the plastic deformation and the transformation behavior at the length scale of interest. This leads to size-dependent results which cannot be obtained using a continuum formulation.

The main findings based on the present simulations are as follows:

- As the ferritic and austenitic grain sizes decrease in multiphase samples of equal composition, the strengthening effect due to smaller grain sizes becomes more important than the strengthening due to martensitic transformation. In samples with larger grains, the load is preferentially carried through the austenitic grains and the transformation-induced plasticity effect is more efficient. It should be noted that this conclusion is based on the present model where the strengthening due to smaller grain sizes is associated to dislocation pile-ups building-up against grain boundaries and phase boundaries that are impenetrable for dislocations; other sources of hardening and, conversely, relaxation mechanisms originating from imperfect interfaces were not investigated.
- Although the mechanism in TRIP steels is referred to as ‘‘transformation-induced plasticity’’, the present simulations indicate that the combination of the two inelastic mechanisms—transformation and plasticity—yields *fewer* dislocations being generated compared to a purely plastic deformation. The appearance of martensitic plates generate more dislocations to accommodate the transformation but, at the same time, it globally reduces the stress level and hence fewer dislocations are generated elsewhere. The effective strength, however, is increased once the transformation rate becomes small.

Since discrete dislocation simulations are (still) computationally expensive for meso- and macroscopic simulations, it is useful from a practical point of view to use the discrete method to develop phenomenological larger-scale relations that can qualitatively capture the lower-scale plastic and transformation behavior. Depending on length scales, such phenomenological relations would correspond to, e.g., plastic and/or transformation hardening laws (such as a modified Hall–Petch relation) that represent the average behavior of the austenite/martensite phase and the average behavior of the ferritic grains. At somewhat larger length scales, the phenomenological relations could represent the average behavior of a mixture of austenite/martensite and ferrite.

In order to establish a macroscopic hardening law for multiphase materials, a rather detailed set of parametric analyses are required to provide a comprehensive view on the small-scale interaction between transformation and plasticity as the deformation evolves. For the ferritic phase, such hardening law would depend on the (inverse) of the grain sizes of the ferrite and the austenite. For the austenite, it would also depend on the (inverse) of the grain sizes of the ferrite and the austenite and, in addition, it would have a non-monotonic dependence on the current value of the austenitic volume fraction. On the other hand, the results shown here suggest that the effect of grain size on a (mesoscale) transformation kinetic law can be

qualitatively reproduced using, e.g., an expression for the energy barrier that is a monotonically decreasing function of the austenitic grain size. Such relation was proposed in an alternative way in Turteltaub and Suiker (2006a), where it was interpreted as a surface energy term that results in a negative contribution to the transformation driving force.

It is worth pointing out that the considerations in this paper are related to strength and not to ductility. Experimental observations reported in Tao et al. (2007) and Yoo et al. (2008) indicate that transformation-induced plasticity in fine-grained structures might improve the ductility. The analysis of this effect requires a fracture model that is outside of the scope of the present work.

Acknowledgment

This research was carried out under project number MC2.03177 in the framework of the Research Program of the Materials innovation institute M2i (http://www.M2i.nl).

References

Ashby, M.F., 1970. Deformation of plastically non-homogenous materials. Philos. Mag. 21, 399–424.
Balint, D.S., Deshpande, V.S., Needleman, A., Van der Giessen, E., 2006. Size effects in uniaxial deformation of single and polycrystals: a discrete dislocation plasticity analysis. Modelling Simul. Mater. Sci. Eng. 14 (3), 409–422.
Balint, D.S., Deshpande, V.S., Needleman, A., Van der Giessen, E., 2008. Discrete dislocation plasticity analysis of the grain size dependence of the flow strength of polycrystals. Int. J. Plasticity 24 (12), 2149–2172.
Ball, J.M., James, R.D., 1987. Fine phase mixtures as minimizers of energy. Arch. Ration. Mech. Anal. 100 (1), 13–52.
Biner, S.B., Morris, J.R., 2002. A two-dimensional discrete dislocation simulation of the effect of grain size on strengthening behavior. Modelling Simul. Mater. Sci. Eng. 10 (6), 617–635.
Biner, S.B., Morris, J.R., 2003. The effect of grain size and dislocation source density on the strengthening behavior of polycrystal: a two-dimensional discrete dislocation simulation. Philos. Mag. 83 (31–34), 3677–3690.
Bowen, P., Druce, S.G., Knott, J.F., 1986. Effects of microstructure on cleavage fracture in pressure-vessel steel. Acta Metall. 34 (6), 1121–1131.
Embury, J.D., 1971. Strengthening Methods in Crystals. Elsevier, Amsterdam.
Eshelby, J.D., Frank, F.C., Nabarro, F.R.N., 1951. The equilibrium of linear arrays of dislocations. Philos. Mag. 42 (327), 351–364.
Hall, E.O., 1951. The deformation and ageing of mild steel: III discussion of results. Proc. Phys. Soc. London B 64, 747–753.
Hirth, J.P., 1972. Influence of grain-boundaries on mechanical properties. Metall. Trans. 3, 3047–3067.
Hirth, J.P., Lothe, J., 1982. Theory of Dislocations. Krieger Publishing Company-John Wiley & Sons, Ltd.
Jacques, P.J., 2004. Transformation-induced plasticity for high strength formable steels. Curr. Opin. Solid State Mater. Sci. 8 (3–4), 259–265.
Jacques, P.J., Ladrière, J., Delannay, F., 2001. On the influence of interactions between phases on the mechanical stability of retained austenite in transformation-induced plasticity multiphase steels. Metall. Mater. Trans. A 32, 2759–2768.
Jacques, P.J., Furnémont, Q., Godet, S., Pardoen, T., Conlon, K.T., Delannay, F., 2006. Micromechanical characterisation of trip-assisted multiphase steels by in situ neutron diffraction. Philos. Mag. 86 (16), 2371–2392.
Jimenez-Melero, E., van Dijk, N.H., Zhao, L., Sietsma, J., Offerman, S.E., Wright, J.P., van der Zwaag, S., 2007a. Martensitic transformation of individual grains in low-alloyed trip steels. Scripta Mater. 56 (5), 421–424.
Jimenez-Melero, E., van Dijk, N.H., Zhao, L., Sietsma, J., Offerman, S.E., Wright, J.P., van der Zwaag, S., 2007b. Characterization of individual retained austenite grains and their stability in low-alloyed TRIP steels. Acta Mater. 55 (20), 6713–6723.
Kocks, U.F., 1970a. Comments on ''yield strength of metals as a function of grain size''. Acta Mater. 7 (2), 1121.
Kocks, U.F., 1970b. Relation between polycrystal deformation and single-crystal deformation. Metall. Trans. 1 (5), 1121.
Mazzoni-Leduc, L., Pardoen, T., Massart, T.J., 2008. Strain gradient plasticity analysis of transformation induced plasticity in multiphase steels. Int. J. Solids Struct. 45 (20), 5397–5418.
Nicola, L., Van der Giessen, E., Needleman, A., 2005. Size effects in polycrystalline thin films analyzed by discrete dislocation plasticity. Thin Solid Films 479 (1–2), 329–338.
Nicola, L., Xiang, Y., Vlassak, J.J., Van der Giessen, E., Needleman, A., 2006. Plastic deformation of freestanding thin films: experiments and modeling. J. Mech. Phys. Solids 54 (10), 2089–21108.
Petch, N.J., 1953. The cleavage strength of polycrystals. J. Iron Steel Inst. 174, 25–28.
Rice, J.R., 1987. Tensile crack tip fields in elastic ideally plastic crystals. Mech. Mater. 6 (4), 317–335.
Shi, J., Turteltaub, S., Van der Giessen, E., Remmers, J.J.C., 2008. A discrete dislocation–transformation model for austenitic single crystals. Modelling Simul. Mater. Sci. Eng. 16 (5).
Suiker, A.S.J., Turteltaub, S., 2005. Computational modelling of plasticity induced by martensitic phase transformations. Int. J. Numer. Meth. Eng. 63, 1655–1693.
Tao, K., Choo, H., Li, H., Clausen, B., Jin, J.-E., Lee, Y.-K., 2007. Transformation-induced plasticity in an ultrafine-grained steel: an in situ neutron diffraction study. Appl. Phys. Lett. 90 (10).
Tjahjanto, D.D., Turteltaub, S., Suiker, A.S.J., van der Zwaag, S., 2006. Modelling of the effects of grain orientation on transformation-induced plasticity in multiphase steels. Modelling Simul. Mater. Sci. Eng. 14, 617–636.
Tjahjanto, D.D., Suiker, A.S.J., Turteltaub, S., Rivera Diaz del Castillo, P.E.J., van der Zwaag, S., 2007. Micromechanical predictions of TRIP steel behavior as a function of microstructural parameters. Comput. Mater. Sci. 41 (1), 107–116.
Tjahjanto, D.D., Turteltaub, S., Suiker, A.S.J., 2008. Crystallographically-based model for transformation-induced plasticity in multiphase carbon steels. Continuum Mech. Therm. 19 (7), 399–422.
Turteltaub, S., Suiker, A.S.J., 2005. Transformation-induced plasticity in ferrous alloys. J. Mech. Phys. Solids 53, 1747–1788.
Turteltaub, S., Suiker, A.S.J., 2006a. Grain size effects in multiphase steels assisted by transformation-induced plasticity. Int. J. Solids Struct. 43, 7322–7336.
Turteltaub, S., Suiker, A.S.J., 2006b. A multi-scale thermomechanical model for cubic to tetragonal martensitic phase transformations. Int. J. Solids Struct. 43, 4509–4545.
Van der Giessen, E., Needleman, A., 1995. Discrete dislocation plasticity: a simple planar model. Modell. Simul. Mater. Sci. Eng. 3 (5), 689–735.
Vitek, V., Mrovec, M., Gröger, R., Bassani, J.L., Racherla, V., Yin, L., 2004. Effects of non-glide stresses on the plastic flow of single and polycrystals of molybdenum. Mater. Sci. Eng. A 387–389, 138–142.
Wechsler, M.S., Lieberman, D.E., Read, T.A., 1953. On the theory of the formation of martensite. Appl. Phys. A Mater. 197 (11), 1503–1515.
Yoo, C.-S., Park, Y.-M., Jung, Y.-S., Lee, Y.-K., 2008. Effect of grain size on transformation-induced plasticity in an ultrafine-grained metastable austenitic steel. Scripta Mater. 59 (1), 71–74.